Electronic Supplementary Material (ESI) for New Journal of Chemistry.

Supporting Information

Controllable Synthesis of Co Nanoparticles in Assistance of Cucurbit[6]uril and its Efficient Photoelectrochemical Catalysis in Water Splitting on a g-C_3N_4 Photoanode

Xin Dai[1], Xian-Yi Jin[1], Rui-Han Gao[1], Qing-Mei Ge[1], Kai Chen[2], Nan Jiang[1], Hang Cong[1,*], Zhu Tao[3], Mao Liu[1,*]

[1]Enterprise Technology Center of Guizhou Province, Guizhou University, Guiyang 550025, China.

Email: hcong@gzu.edu.cn for H. Cong, liumao@outlook.com for M. Liu.

[2]Collaborative Innovation Center of Atmospheric Environment and Equipment Technology, Jiangsu Key Laboratory of Atmospheric Environment Monitoring and Pollution Control, School of Environmental Science and Engineering, Nanjing University of Information Science & Technology, Nanjing, 210044, China

[3]Key Laboratory of Macrocyclic and Supramolecular Chemistry of Guizhou Province, Guizhou University, Guiyang 550025, China.

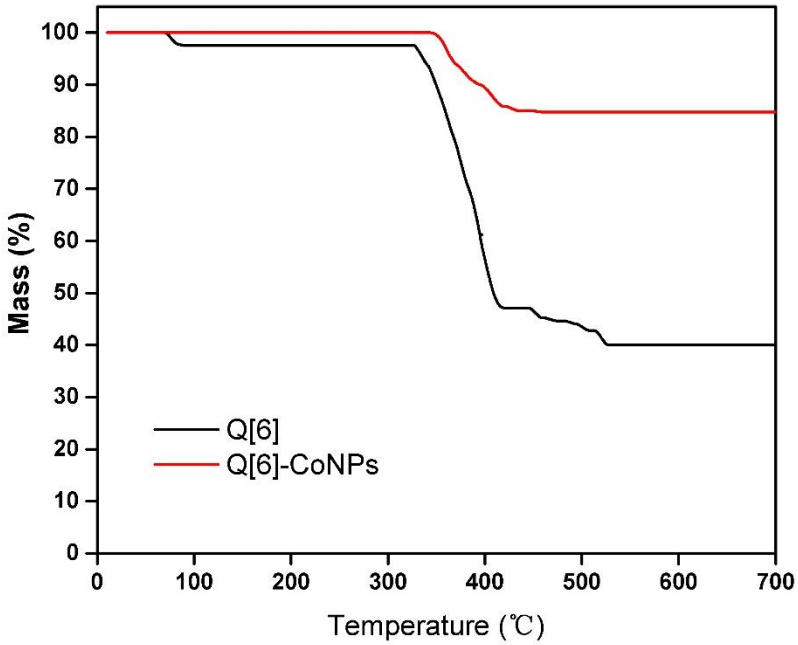

Figure S1. TG curves of Q[6] and Q[6]-Co NPs

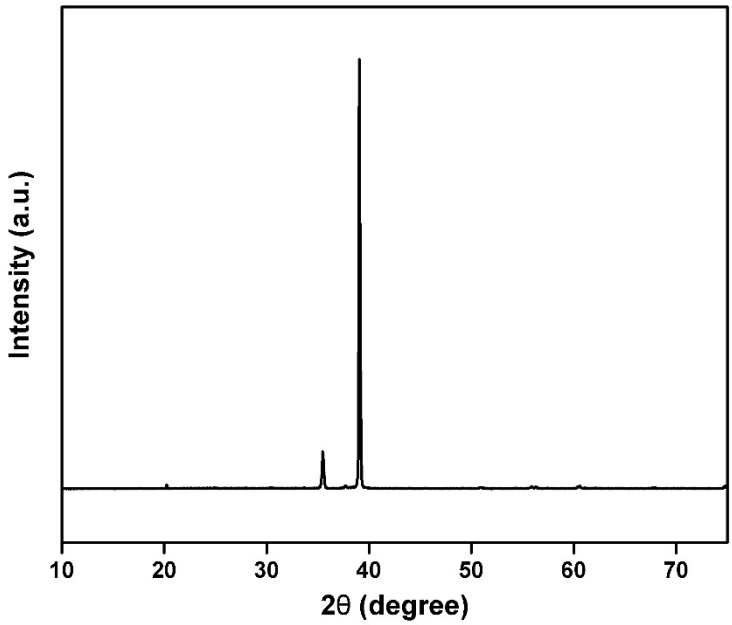

Figure S2. XRD pattern of the Q[6]

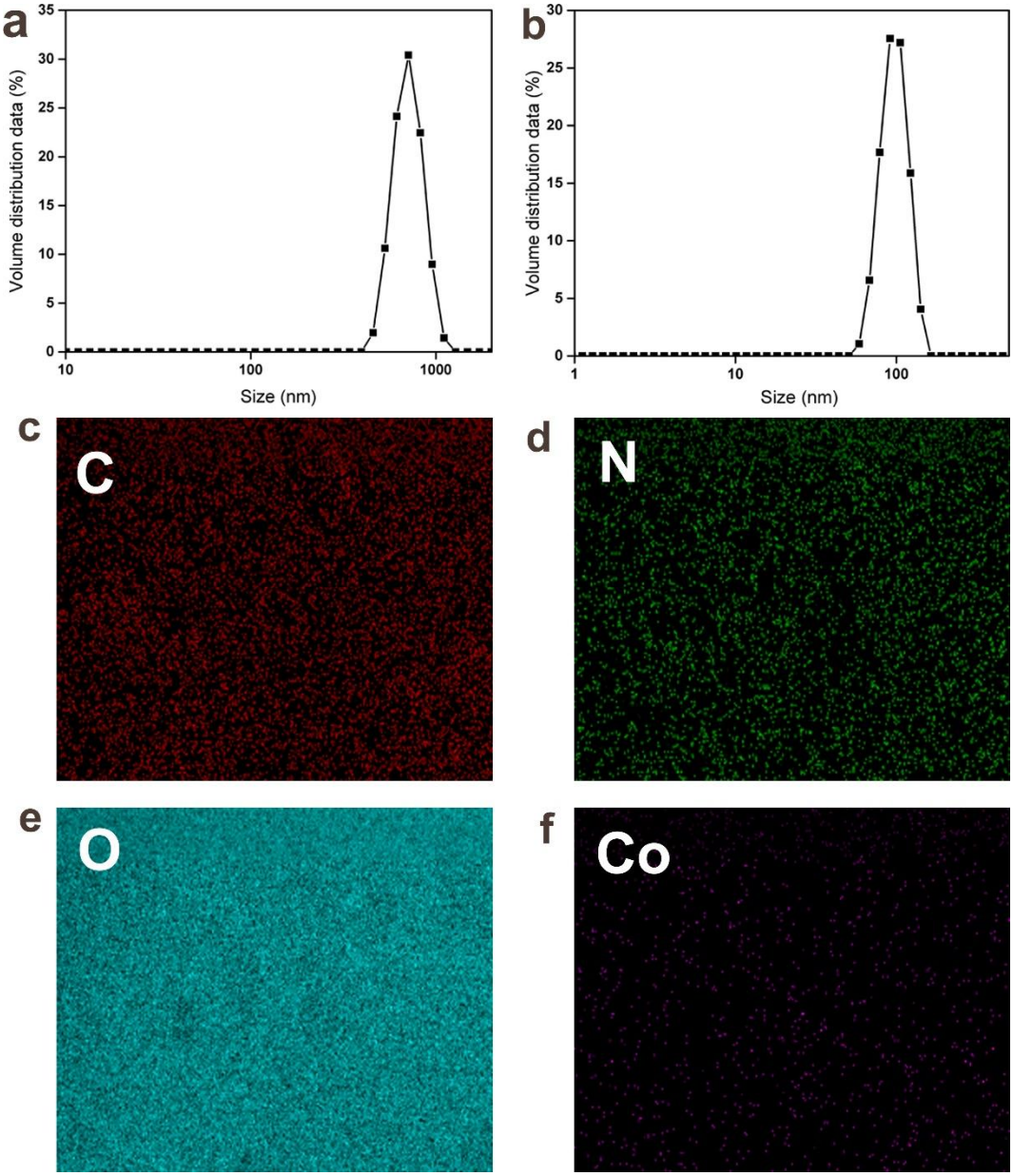

Figure S3. Size distribution of (a) Co NPs and (b) Q[6]- Co NPs; Elemental mapping image of Q[6]-Co NPs showing the element distributions of (c) C; (d) N; (e) O; (f) Co.

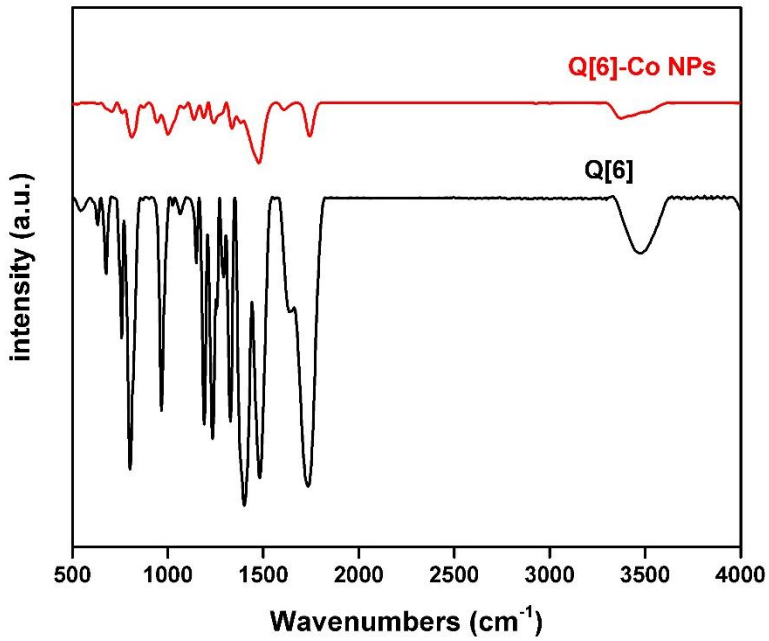

Figure S4. The infrared spectroscopy (IR) spectra of Q[6] and Q[6]-CoNPs.

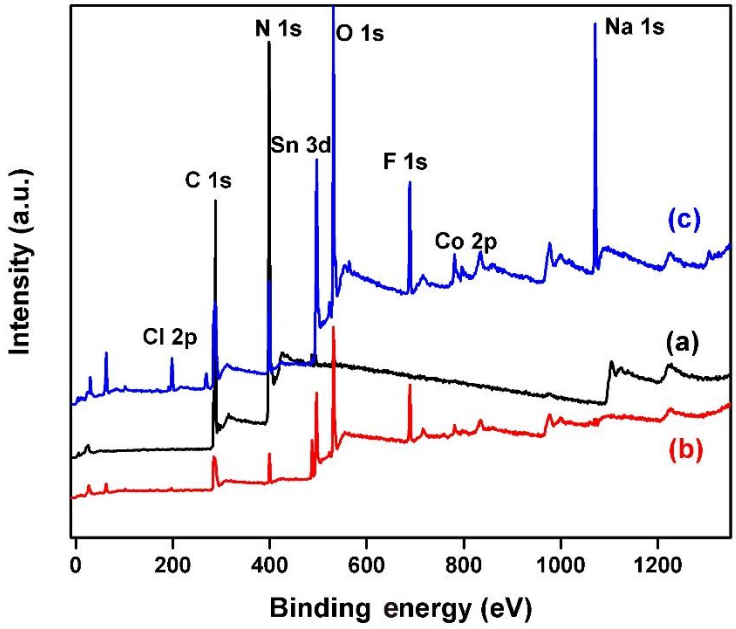

Figure S5. XPS survey spectra of (a) g-C_3N_4; (b) Q[6]-Co NPs; (c) g-C_3N_4/Q[6]-Co NPs.

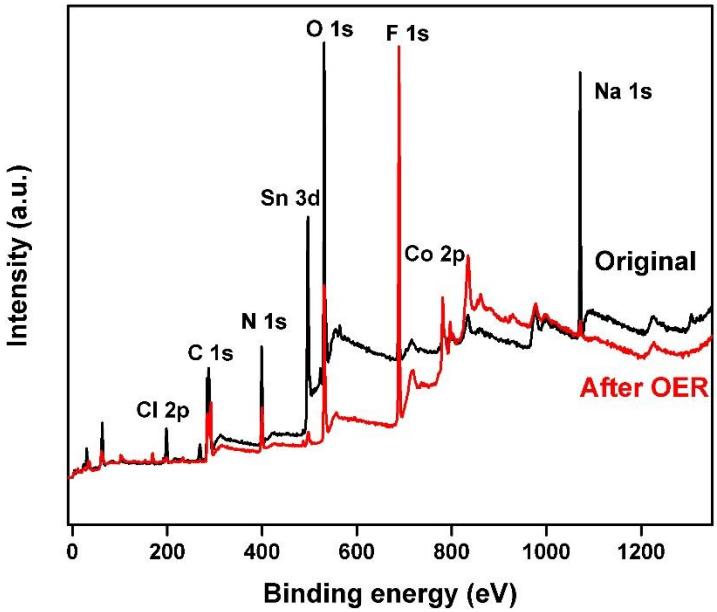

Figure S6. XPS survey spectra of g-C_3N_4/Q[6]-Co NPs photoanode before and after OER reaction.

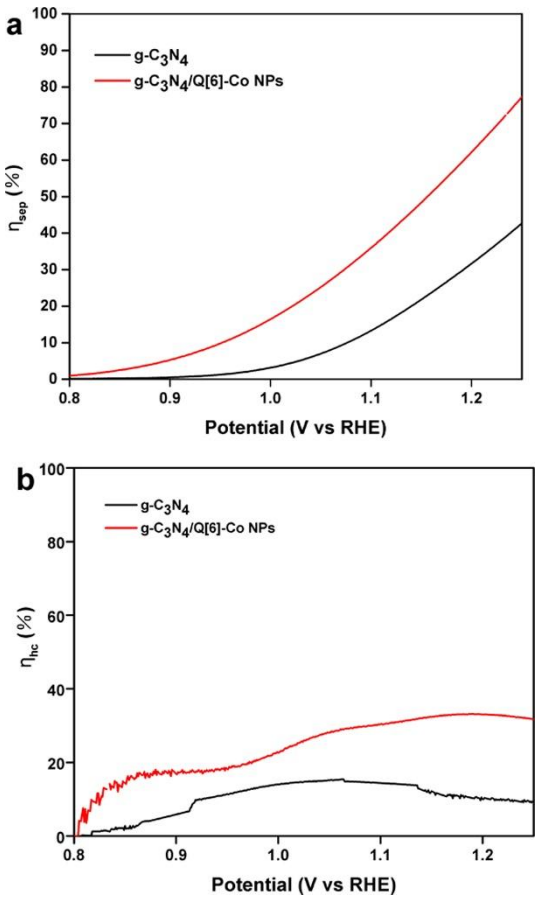

Figure S7. (a) η_{sep} and (b) η_{hc} of the g-C_3N_4 and g-C_3N_4/Q[6]-Co NPs photoelectrodes using Na_2SO_3 as the hole scavenger

The charge separation efficiency (η_{sep}) and hole collection efficiency (η_{hc}) were measured by hole scavengers to assess the separation of electron/holes. Light absorption efficiency (η_{abs}) can be expressed as (1), Where $A_{(\lambda)}$ is absorbance, λ is the wavelength. where the J_{max} is maximum photocurrent density achievable assuming 100% incident photon-to-current conversion efficiency for photons with energy higher than the band gap.

$$\eta_{abs} = 1\text{-}10^{-A(\lambda)} \qquad (1)$$

$$\eta_{sep} = J_{Na_2SO_3} / J_{max} \cdot \eta_{abs} \qquad (2)$$

$$\eta_{hc} = J_{H_2O} / J_{Na_2SO_3} \qquad (3)$$

The charge separation and hole collection efficiencies of the pure g-C_3N_4 and g-C_3N_4/Q[6]-Co NPs photoanodes were shown in Figure S7a and S7b, respectively. The onset potential of g-C_3N_4/Q[6]-Co NPs had a negative shift relative to bare g-C_3N_4, which was owing to the addition of a hole sacrificial agent in the electrolyte accelerated the reaction kinetics of the holes and reduced the recombination rate of the surface charge of the semiconductor electrode so that the photoelectrode could react at a lower potential and generate an obvious photocurrent. Moreover,

the η_{sep} and η_{hc} of g-C_3N_4/Q[6]-Co NPs were 71.29% and 32.42% at 1.23 V vs. RHE, which were 1.9 and 3.3 times higher than that of pure g-C_3N_4 (38.30% and 9.70% at 1.23 V vs. RHE), respectively. The aforementioned results indicated that the tight combination of g-C_3N_4 film and Q[6]-Co NPs was more conducive to reducing carrier recombination and accelerating the transfer of charge at the electrode/electrolyte interface to promote the oxygen evolution reaction kinetics, which was also consistent with the EIS result (Figure 5a).

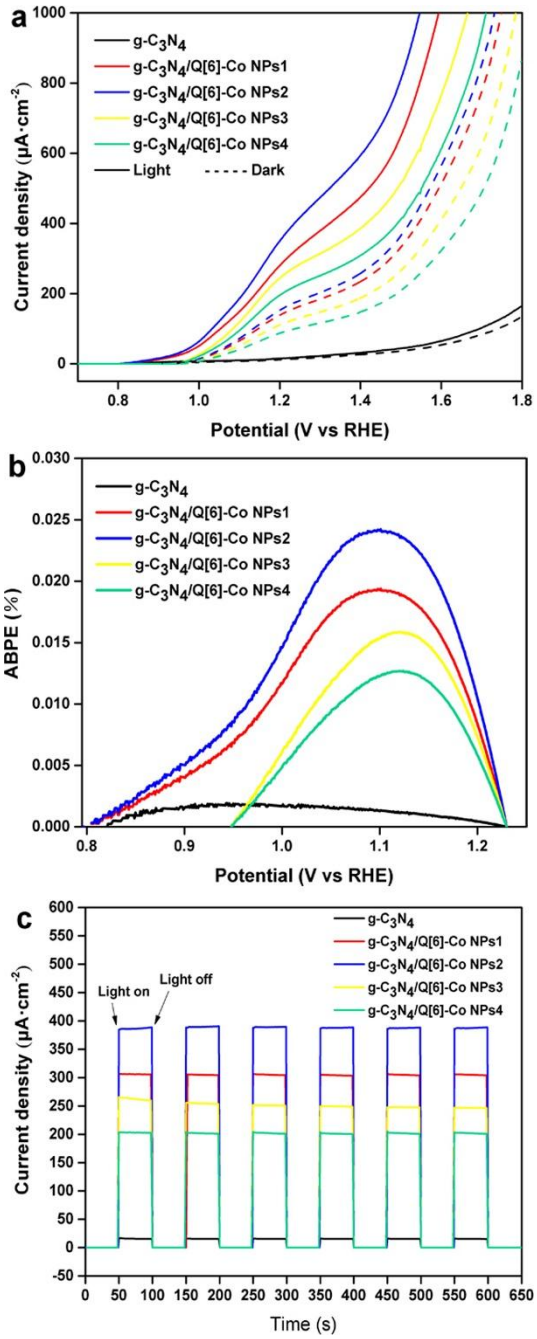

Figure S8 (a) LSV curves of the as-prepared photoanodes under light illumination (solid lines) and dark (dashed lines) in 0.5 M Na_2SO_4 solution; (b) Plots of ABPE (%) vs. applied potential obtained for all photoanodes in 0.5 M Na_2SO_4 solution; (c) Chronoamperometric *I-t* curves of all photoanodes under chopped illumination at 1.23 V vs. RHE in 0.5 M Na_2SO_4 solution.

Keeping the mass of g-C_3N_4 constant, we obtained g-C_3N_4/Q[6]-Co NPs (g-C_3N_4/Q[6]-Co NPs1, g-C_3N_4/Q[6]-Co NPs2, g-C_3N_4/Q[6]-Co NPs3 and g-C_3N_4/Q[6]-Co NPs4) catalysts with different Q[6]-Co NPs contents, as the mole ratios of 1:1, 1:2, 1:3 and 1:4, respectively. In Figure S8a, g-C_3N_4/Q[6]-Co NPs1, g-C_3N_4/Q[6]-Co NPs2, g-C_3N_4/Q[6]-Co NPs3 and g-C_3N_4/Q[6]-Co NPs4 photoelectrodes showed photocurrent densities of 314, 393, 270 and 216 μA·cm^{-2} at 1.23 V vs. RHE, respectively. Compared with these samples, the g-C_3N_4/Q[6]-Co NPs2 photoelectrode had a more efficient PEC performance, which was over 23 times higher than the pristine g-C_3N_4

(17 $\mu A \cdot cm^{-2}$). Presumably, the aforementioned results could be due to the following reasons: after incorporating Q[6]-Co NPs on g-C_3N_4, when the molar mass ratio of g-C_3N_4 to Q[6]-Co NPs was less than 1:2, the formed semiconductor–metal junction during the Fermi level equilibration contributed to the enhanced photoelectrochemical performance of g-C_3N_4/Q[6]-Co NPs. However, when the molar ratio exceeded 1:2, the decrease in photocurrent density may be due to the excessive Q[6]-Co NPs occupying the active sites and shielding of the light absorption.

Compared with g-C_3N_4, all composite photoelectrodes had significantly higher peak ABPE values in the order of: g-C_3N_4/Q[6]-Co NPs2 (0.0242%) > g-C_3N_4/Q[6]-Co NPs1 (0.0194%) > g-C_3N_4/Q[6]-Co NPs3 (0.0159%) > g-C_3N_4/Q[6]-Co NPs4 (0.0126%) (Figure S8b). As expected, g-C_3N_4/Q[6]-Co NPs2 possessed a maximum photoconversion efficiency, which was 12.6 times higher than that of bare g-C_3N_4 (0.00193%). In Figure S8c, the observed steady-state photocurrent density of g-C_3N_4/Q[6]-Co NPs2 was higher than those of g-C_3N_4/Q[6]-Co NPs1, g-C_3N_4/Q[6]-Co NPs3, g-C_3N_4/Q[6]-Co NPs4 and pure g-C_3N_4, which was consistent with the LSV results as shown in Figure S8a.

Table S1. Crystal Data and Structure Refinements for 1

Compound	**1**		
chemical formula	$C_{36}H_{36}N_{24}O_{20}Co_2Cl_4$	Volume /Å^3	2740(3)
formula weight	1384.55	Z	2
crystal system	Monoclinic	D_c /g cm^{-3}	1.678
space group	*C 2/m*	μ /mm^{-1}	0.897
a /Å	20.723(13)	F(000)	1404
b /Å	13.892(9)	reflections collected/unique	2773/2271
c /Å	11.255(7)	data / restraints / parameters	2773/0/205
α /°	90	GOF	1.093
β /°	122.265(9)	R_1, wR_2 [$I > 2\sigma(I)$][a,b]	R_1 = 0.1905, wR_2 = 0.4269
γ /°	90	R_1, wR_2 (all data)	R_1 = 0.2015, wR_2 = 0.4299
temperature /K	293(2)		

[a]$R_1 = \Sigma||F_o| - |F_c||/\Sigma|F_o|$. [b]$wR_2 = |\Sigma w(|F_o|^2 - |F_c|^2)|/\Sigma|w(F_o)^2|^{1/2}$, where $w = 1/[\mathrm{s}^2(F_o^2) + (aP)^2 + bP]$. $P = (F_o^2 + 2F_c^2)/3$

Table S2. The R_s and R_{ct} of all samples extracted from fitting electrochemical impedance spectra under illumination

Photoanodes	R_s / Ω	R_{ct} / Ω
g-C_3N_4	18.50	26.80
g-C_3N_4/ Q[6]-Co NPs	10.13	1.45

Table S3. The R_s and R_{ct} of the different catalysts extracted from fitting electrochemical impedance spectra under dark

Photoanodes	R_s / Ω	R_{ct} / Ω
g-C_3N_4	22	31.5
g-C_3N_4/ Q[6]-Co NPs	9.62	1.78